J. Fluid Mech. (1979), *vol.* 93, *part* 4, *pp.* 631-659
Printed in Great Britain

Relaxing wakes behind surface-mounted obstacles in rough wall boundary layers

By I. P. CASTRO

Department of Mechanical Engineering, University of Surrey

(Received 15 November 1978)

Detailed measurements in the wakes behind two-dimensional square section blocks (height h) mounted in thick rough wall boundary layers (height δ) are presented for cases in which $h/\delta \ll 1$. The data provides some insight into the relaxing flow downstream of reattachment, confirming the conclusion of Bradshaw & Wong (1972) that reattaching flows are surprisingly complicated and involve considerable distortion of the separated shear layer. In particular, the measurements show that eddy length scales are considerably reduced and, since the flow eventually relaxes to a boundary layer similar to that upstream, turbulence models based on eddy viscosity concepts cannot, in principle, be expected to be satisfactory. Using the present data this is demonstrated by a more detailed comparison with the theoretical predictions of Counihan, Hunt & Jackson (1974) than has been previously possible. It is shown that, whilst their theory does not predict the behaviour of the turbulent stresses, it does give reasonable agreement with the mean velocity perturbations at least in the near wake $-10 < x/h < 30$. Except in the near wall region, where the roughness provides the dominant length scale, it is argued that the rate at which the perturbation flow decays is governed largely by the amount by which the separated shear layer is distorted prior to reattachment, which in turn is determined by, say, a turbulence Reynolds number of the body, $(hU/\nu_0)_h$, or, in other words, by the characteristics of the upstream flow at, say, the body height.

1. Introduction

'At present little is known about the wake behind surface obstacles in turbulent boundary layers'; so wrote Counihan *et al.* (1974) in the introduction to their theoretical work on such wakes behind two-dimensional bodies. Despite their rather limited experimental work, undertaken as a test of the theory, it seems that the truth of their statement has altered only marginally for two-dimensional bodies, although some useful measurements behind three-dimensional bodies have since been reported (e.g. Peterka & Cermak 1975; Castro & Robins 1977). The theory developed by Counihan *et al.* (1974), hereafter known as CHJ, was recognized to be fairly primitive but, partly in view of the lack of detailed experimental data, it has not seemed worthwhile attempting any major improvements (Hunt, private communication). The present work was undertaken as a more detailed test of the theory and, perhaps more importantly, as an attempt to investigate directly the effects, on the decay and turbulence structure of the wake, of varying parameters like h/δ (where $h/\delta \ll 1$) and the roughness of the boundary. For simplicity the investigation was limited to the wake flow

0022-1120/79/4269-7260 $02.00

produced by square section two-dimensional blocks immersed in thick rough-wall boundary layers; it is hoped eventually to investigate the effect of gradually reducing the width (span) of the body towards the previously investigated 'limiting' case of a cube (Castro & Robins 1977).

Townsend (1965) has also given a theory for two-dimensional wall wakes, but he was concerned primarily with a change in wall boundary conditions so, as CHJ pointed out, his analysis is only valid for bodies so much smaller than the height of the constant stress layer that they introduce no new length scale effects which remain significant far downstream. It cannot therefore be reasonably expected to apply to the present case.

Although the only previously reported detailed turbulence measurements in the wake of two-dimensional bodies on rough surfaces are believed to be those of CHJ, there have been some more comprehensive measurements of flow down a rearward facing step (Bradshaw & Wong 1972; Chandrsuda 1975; Baker 1977; Etheridge & Kemp 1978). The relaxing flow downstream of reattachment might be expected to have, at least in some respects, similar features in the two cases so that the present data are compared with available step flow data where relevant.

Now that numerical techniques for predicting recirculating flows are available some workers are attempting to calculate flows like those investigated here. For example, Shieh, Frost & Bitte (1976) have recently reported a numerical study of neutrally stable atmospheric flow over a two-dimensional block, but they were clearly hampered in their analysis of the predictions by a lack of sufficiently detailed experimental data. The present results should be useful in providing a set of data against which to test prediction methods. However, the large effects of extra strain rates on turbulence structure are by now well known (e.g. Bradshaw 1975) so that, apart from serious numerical difficulties, chiefly regarding accuracy in elliptic flow regions, which have not been properly surmounted (Castro 1978*a*, 1979), the common turbulence models used in such predictions are not likely to be adequate for such complicated flows. In that they provide some further insight into the turbulence structure of this particular class of complex flow, the present results should also be useful in the ongoing task of developing better turbulence models, although it must be emphasized that more detailed experiments, particularly in the regions just upstream and downstream of the body, may be required for a totally adequate understanding of the flow.

The following section describes the basic experimental arrangements and includes details of the rough wall boundary layers used along with an introduction to the particular flows investigated. A typical selection of the data for these flows is presented in § 3 which leads naturally to a more detailed comparison of the results with the CHJ theory ia § 4. In addition to extensive measurements of mean velocity and Reynolds stresses in the wakes some more limited measurements of turbulence length scales were made; these, along with the more basic measurements, are used in § 5 in a further assessment of the assumptions used in the theory and, indeed, of some of the more common turbulence models used in numerical prediction methods.

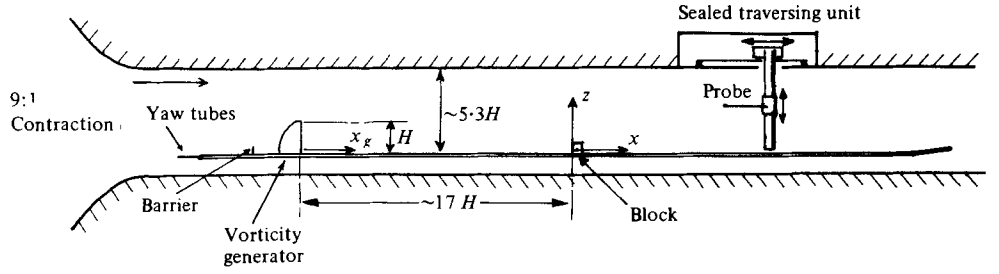

FIGURE 1. Sketch of the experimental arrangement (not to scale).

2. Experimental arrangements

2.1. *General details*

All the experiments were undertaken in the $6 \times 0{\cdot}9 \times 0{\cdot}75$ m suck-down wind tunnel at Marchwood Engineering Laboratories. In the empty working section mean velocity variations were less than $\pm \frac{1}{4}\%$ and the longitudinal turbulence intensity was less than $0{\cdot}05\%$. A false floor spanning the 0·9 m horizontal width of the tunnel and extending down most of the working section length was installed about 100 mm above the floor. It was equipped with an adjustable flap at the rear and calibrated yaw tubes at the nose to enable zero circulation to be maintained in all the flows studied. A castellated barrier wall, vorticity generators and distributed surface roughness were used to generate thick turbulent boundary layers on the false floor (figure 1). The general details of such a system have been discussed elsewhere (Counihan 1969; Robins 1979) and the particular details of the two boundary layers used in the present study are described by Castro (1978*b*). Basic flow characteristics are presented in § 2.2 and further details mentioned as necessary.

Mean velocity and turbulence measurements were made with Pitot tubes, single and crossed hot-wire anemometers and, occasionally, a pulsed-wire anemometer. The probes were mounted on an automated two-directional traversing mechanism with a digital readout permitting repositioning of the probes to within 0·1 mm at worst. Hatches in the working section roof allowed the traversing gear to be positioned anywhere down the length of the working section and its orientation could be easily changed to enable continuous traversing in either the axial or the spanwise direction in addition to the permanent vertical traverse.

The anemometer bridge outputs were passed through low pass filters set at about 20 kHz to reduce noise, backed off with an accurately known d.c. voltage, amplified and then digitized immediately; the resulting data were analysed on-line using an Interdata Model 74 Minicomputer which, in fact, controlled the digitization rate. Fortran routines were written to analyse each data point sequentially before requesting the next. Hot-wire calibrations, including yaw response calibrations for crossed-wire probes using a cosine fit (Bradshaw 1971), were also carried out on-line and the measurement procedure included linearization of each sample with running calculations of mean velocity and Reynolds stresses and, optionally, triple products and probability density distributions. The software was sufficiently fast to allow a complete crossed-wire traverse of, say, 10 points with 2000–4000 samples of each wire voltage at each point and calibrations before and after the traverse to be completed within

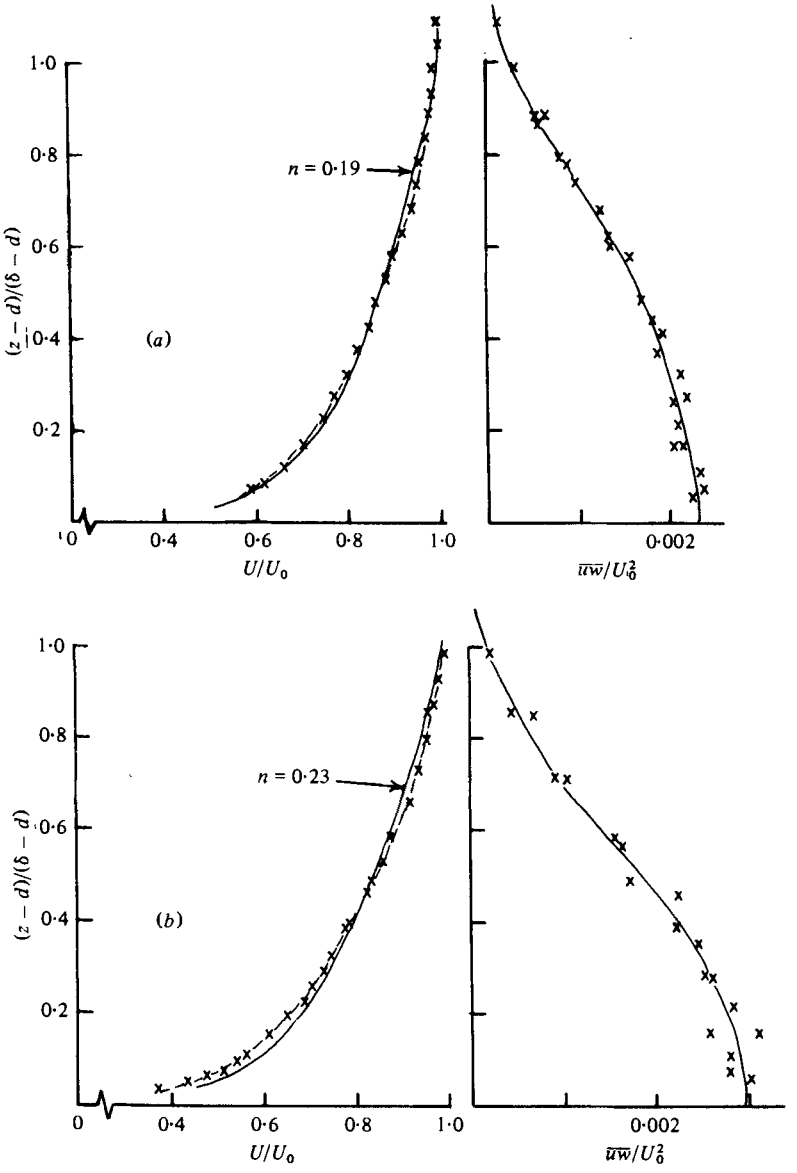

FIGURE 2. Mean velocity and shear stress: (*a*) BL1; (*b*) BL2.

about half an hour, each set of samples effectively requiring an integration time of 1–2 min. Little problem with hot-wire drift was therefore experienced, but if velocities measured before and after a run did differ by more than about $\frac{1}{2}\%$ the complete traverse was rejected.

For determination of the dissipation length scale, $L = \overline{uw}^{\frac{3}{2}}/\epsilon$, where ϵ is the turbulence dissipation rate, spectral measurements were made with a single hot wire and an analogue spectrum analyser. This latter was carefully calibrated and measurements were concentrated in the wavenumber region expected to contain the inertial subrange. The data were fitted to the well-known universal spectrum, defined in the inertial

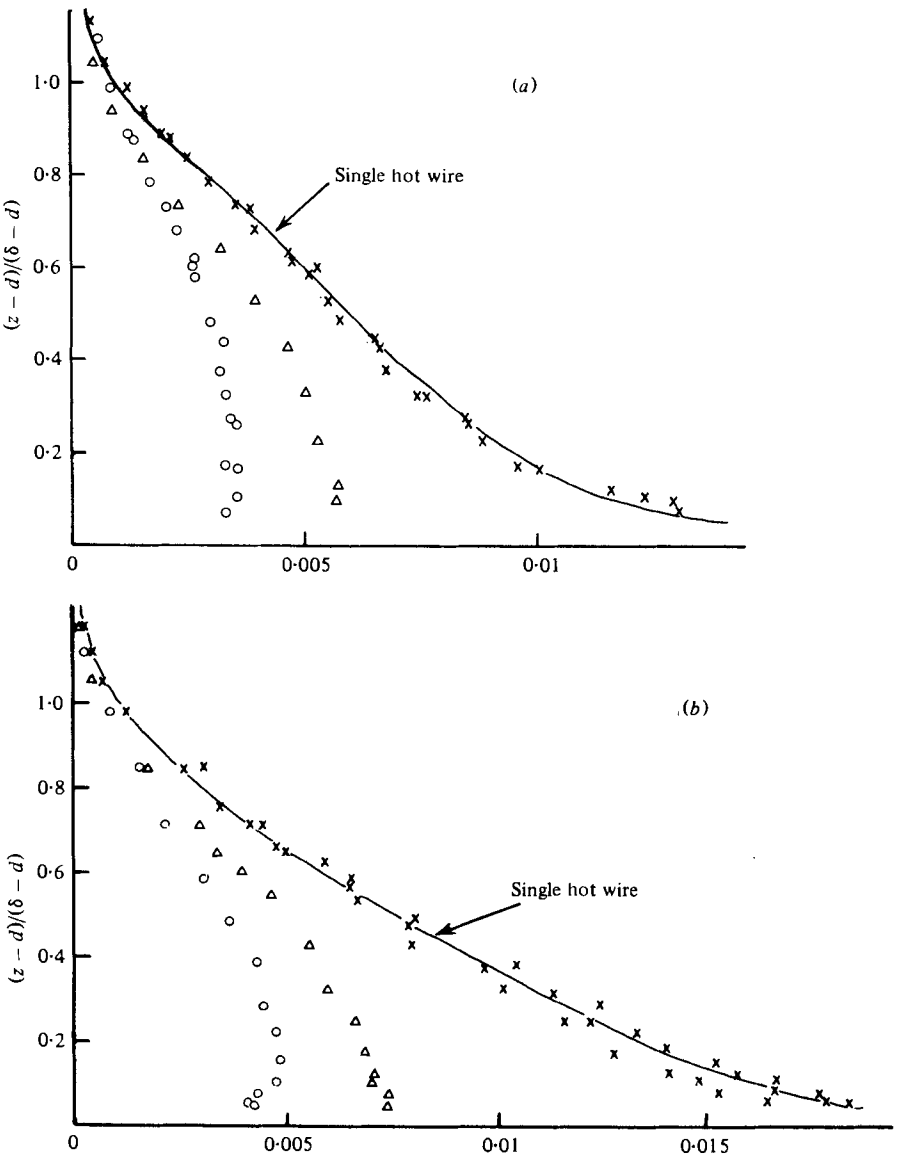

FIGURE 3. Normal turbulent stresses; ×, $\overline{u^2}/U_0^2$; ○, $\overline{w^2}/U_0^2$; △, $\overline{v^2}/U_0^2$; ——, single wire results; (*a*) BL1; (*b*) BL2.

subrange by $\phi(k) = A\epsilon^{\frac{2}{3}}k^{-\frac{5}{3}}$, where ϕ is the spectral density of $\overline{u^2}$ at wavenumber k, with A taken as 0·53, consistent with the suggestions of Lawn (1971) and Bradshaw (1969). Values for e, and hence L, followed from this fit. Such measurements of ϵ are not likely to be too precise, but they are probably no more inaccurate than those obtained in other ways and since the same technique was used for the L measurements in the undisturbed boundary layer are quite adequate for the present purposes.

Two pressure-tapped square-section blocks of side 12 and 25 mm were constructed from sheet brass; particular care was taken to obtain sharp corners and, by using hypodermic tubing inlaid diagonally in the block surfaces and subsequently drilled,

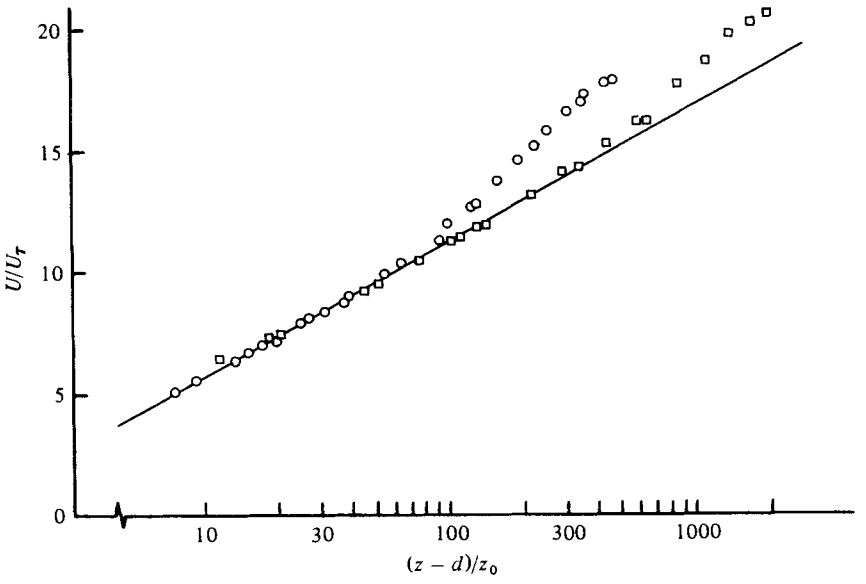

FIGURE 4. Logarithmic-law mean velocity profiles at $x_g/H \simeq 17$. □, BL1; ○, BL2; ——, $U/U_\tau = \kappa^{-1}\ln[(z-d)/z_0]$, $\kappa = 0{\cdot}41$.

it was possible to obtain an adequate number of pressure tappings without having to use too many separate tubes. All pressures were measured using a capacitance type transducer and an integrating digital voltmeter. Since nearly all measurements were normalized it was only necessary to ensure good linearity of the pressure transducer.

2.2. The boundary layers

The present work utilized two boundary layers, designated BL1 and BL2, both of which were generated using a set of vorticity generators 122 mm in height (H), with an upstream barrier wall of height b, given by $b/H = 0{\cdot}15$. For BL1 the wall roughness was Lego baseboard and for BL2 the roughness was increased by covering 25 % of the surface area with regularly distributed Lego 'slimbricks' ($16 \times 8 \times 3{\cdot}2$ mm in height).

Both boundary layers exhibited approximate similarity beyond about $x_g/H = 12{\cdot}0$, where x_g is measured from the vorticity generators, and the normalized profiles of mean velocity and Reynolds stresses are shown in figures 2 and 3. Figure 4 shows the mean velocity data plotted in log-law form and compared with the familiar universal distribution

$$\frac{U}{U_\tau} = \frac{1}{\kappa}\ln\left(\frac{z-d}{z_0}\right),$$

where U_τ is the friction velocity, z_0 is the roughness length, d is the zero-plane displacement and κ is von Kármán's constant, taken as 0·41. It is apparent that the wake component of BL1 (0·38) is rather weaker than that of BL2 (0·47) which is itself less than the standard Coles (1956) value of the wake parameter $\Pi(0{\cdot}55)$ for developed zero pressure gradient boundary layers. This seems to be a general feature of boundary layers generated in this way but, for the present purposes, is not significant since $h/\delta \ll 1$. For a discussion of the development process see Robins (1979) and, for BL1 and BL2 in particular, Castro (1978*b*).

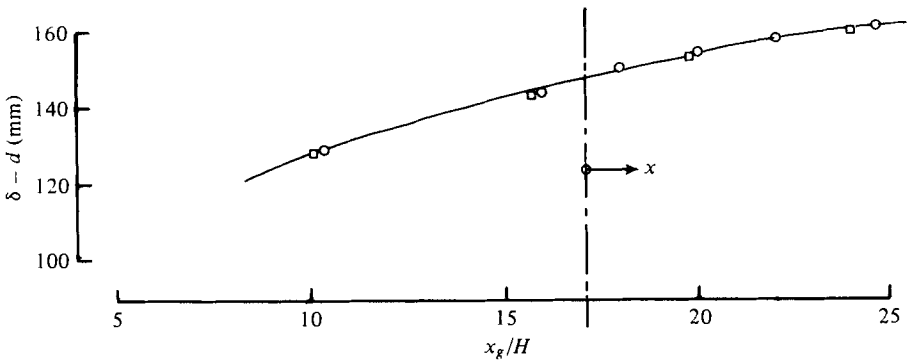

FIGURE 5. Boundary-layer growth. □, BL1; ○, BL2.

Flow	d (mm)	z_0 (mm)	U_τ/U_0	n
BL1	~1·8	0·071	0·048	0·19
BL2	~4·0	0·32	0·055	0·23

TABLE 1

Flow	Upstream boundary layer	Nominal h (mm)	h/z_0	h/δ	$(U/U_0)_h$	$K \equiv \frac{2\nu_0(h)}{hU(h)}$	$\frac{\tilde{C}}{h^2U(h)^2}$
F1L	BL1	25	327	0·157	0·685	0·045	0·825
F2L	BL2	25	78	0·169	0·625	0·049	0·76
F1S	BL1	12	144	0·069	0·580	0·068	0·82

TABLE 2. Various parameters for the three flows.

Figure 5 shows the growth of the boundary-layer thickness, δ, defined as the location at which the mean velocity is 0·99 of its free-stream value, and table 1 summarizes the basic characteristics of the developed layers. n in table 1 and figure 2 is the exponent giving the most reasonable fit of a mean velocity power law profile to the experimental data.

2.3. *The flows investigated*

Three flows, designated F1L, F1S and F2L, were investigated. For F1L and F2L the larger of the two blocks (25 mm) was placed 17·1 vorticity generator heights downstream of the generators in BL1 and BL2, respectively, and for F1S the smaller block (12 mm) was mounted at the same position in BL1. The appropriate values of h/z_0, h/δ and $(U/U_0)_h$ are given in table 2 along with some other basic flow parameters introduced later. Only for F1S was the block totally submerged in the log-law (constant stress) region; in the other two cases the top of the block was just outside, although still of course deep within the fully turbulent flow – the maximum h/δ was only about 0·17. In table 2 and all subsequent figures the appropriate zero plane displacement, d, has been subtracted from h and δ (and all vertical heights).

Spanwise measurements at $x_g/H = 20$ showed that the boundary layers were

closely two-dimensional over a span equal to at least four boundary-layer thicknesses (about $\frac{2}{3}$ of the total tunnel width). For the largest block this was equivalent to about 24 block heights and since, in addition, spanwise variations of block surface pressure coefficients were found to be less than $\pm 1\frac{1}{2}\%$ over the same central span, the use of end-plates was considered unnecessary. It is probable that for nominally two-dimensional bodies with sharp edges the three-dimensional end effects are less significant than for bodies (like circular cylinders) whose geometry does not impose fixed and straight separation lines.

For most of the tests the Reynolds number based on free-stream velocity and the body height was about $1{\cdot}5 \times 10^4$ or, for the smaller body, about half this value. It was found that any Reynolds number sensitivity in the flow, for

$$0{\cdot}5 \times 10^4 \lesssim Re \lesssim 2 \times 10^4,$$

was marginal and not really distinguishable from the general measurement scatter.

CHJ showed how the obstacle wake flow was related to the pressure field close to the body and suggested that future experiments should include measurements of the pressures on the surface, in addition to those on the obstacle. However they also showed that small errors in such measurements could lead to large errors in the estimation of, say, the combined couple on the surface and the obstacle. Since it was difficult to see how accurate and meaningful measurements of static pressure on a rough surface could be made, and since the dynamics of the wake flow is undoubtedly the more interesting and useful aspect of the study, such measurements were not attempted in the present work.

Apart from the block surface pressures, most of the work was concentrated on the wake flow downstream of reattachment. Measurements of vertical profiles of mean velocity, shear stress and all three components of normal stress were made at a minimum of ten downstream locations between x/h of 10 and 60, where x is measured from the front face of the block. Less extensive measurements of the turbulence dissipation rate and some velocity probability density distributions were also made.

3. Experimental results

3.1. *Block surface pressures*

Figure 6 shows the static pressure variations on the block surfaces for all three cases. The coefficients have been normalized according to

$$C_p = (p - p_0)/\tfrac{1}{2}\rho U_0^2,$$

where p_0 and $\frac{1}{2}\rho U_0^2$ are the static and dynamic free-stream pressures measured at the block position but in its absence and at the same tunnel reference velocity (the contraction exit velocity) used for the main tests.

As h/z_0 decreases it is clear that the surface pressures decrease in magnitude so that the body forces (drag and overturning moment) decrease, as expected. It is also apparent that there is a significant pressure recovery on the top surface. Whilst this is not so marked as it is in the case of a cube mounted in a thick boundary layer with similar h/δ (Castro & Robins 1977), it is indicative of at least attempted reattachment of the separated shear layer. Flow visualization and some quantitative measurements with a pulsed-wire anemometer placed just downstream of the top rear edge of the

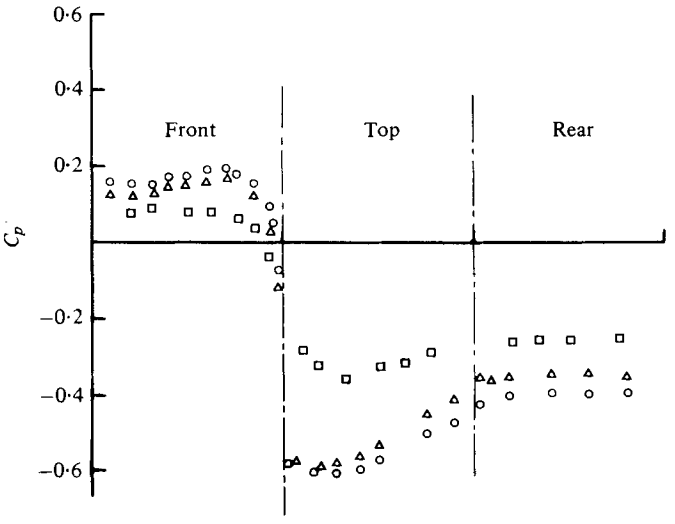

FIGURE 6. Block surface pressures. ○, F1L; △, F2L; □, F1S.

blocks confirmed that reattachment did occur as it did in the experiments of CHJ. Inspection of the pulsed wire anemometer signals showed that only very occasionally did the instantaneous velocity become negative at a location just above and behind the top rear edge of the block. Whilst it is possible that these occurrences resulted from a momentary lack of shear layer reattachment, it is more likely that they were simply a consequence of the locally high level of turbulence intensity. This is interesting because previous work has indicated that, for a surface-mounted block in a smooth wall boundary layer, with $\delta/h \sim 9{\cdot}3$, the separated shear layer did not reattach onto the body (Castro & Fackrell 1978). In that case the upstream turbulence intensity at, say, the block height, although considerably higher than it would be in the case of *thin* upstream boundary layers (cf. Crabb, Durão & Whitelaw 1977) was rather lower than it was in the present case. Clearly a quantitative understanding of the turbulence characteristics necessary to promote reattachment on the top surface of a surface-mounted two-dimensional block, along with the effect of h/D, where D is the axial length of the body, requires further study. The indications are, however, that for square-section bodies ($h/D \sim 1$) of 'building' height in neutrally stable atmospheric boundary layers shear layer reattachment onto the body surface is likely. This fact, incidentally, has obvious implications for those concerned with the size and siting of gaseous effluent dispersal vents or chimney stacks. It also means, of course, that the overall body forces are rather lower than they would be if the shear layer did not reattach.

For the present flows, table 3 gives the values of the drag coefficients, obtained by integrating the surface pressure distributions shown in figure 6. Whilst the wake flow is, according to CHJ, more closely connected with the couple on the body than its drag, these data are nevertheless significant. Included in the table are values of the drag coefficients normalized by the wall friction velocity, U_τ, rather than U_0, and the parameter $1/K$ which is used in the theory of CHJ and is defined by

$$1/K = hU(h)/2\nu_0(h),$$

Flow	$1/K$	C_D	C_{D_T}	h/z_0	$\frac{C}{\rho h^2 U(h)^2}$	$\frac{\tilde{C}}{h^2 U(h)^2}$
F1L	222	0·55	238	327	0·28	0·825
F2L	204	0·475	157	78	0·24	0·75
F1S	147	0·31	135	144	0·16	0·82

TABLE 3. Body forces for the three flows.

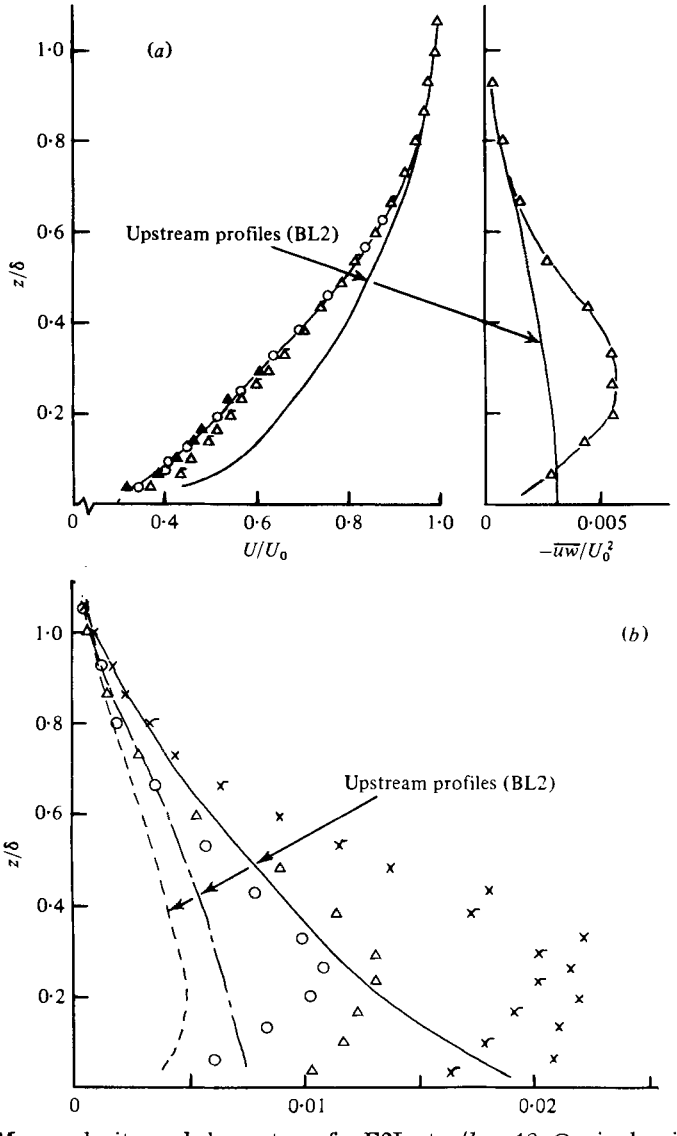

FIGURE 7. (*a*) Mean velocity and shear stress for F2L at $x/h = 18$. ○, single wire; △, crossed wire in the x, z plane (△) and the y, z plane (△). ▲, corrected crossed wire. (*b*) Normal turbulent stresses for F2L at $x/h = 18$. × (x, z plane), ×̄ (y, z plane). $\overline{u^2}/U_0^2$; △, $\overline{v^2}/U_0^2$; ○, $\overline{w^2}/U_0^2$.

where $\nu_0(h)$ is the eddy viscosity in the undisturbed boundary layer at the block height. This is equivalent to a turbulent 'Reynolds number' of the obstacle. A number of workers have sought to correlate the drag of bluff obstacles (usually fences) in boundary layers with various parameters of the upstream flow. Plate (1964), for example, attempted a correlation between the drag of fences on smooth walls and δ/h whereas Good & Joubert (1968) showed that the drag apparently also depends on the wall friction velocity (unless $h/\delta \gg 1$). More recently Raju, Loeser & Plate (1976) have suggested that the drag correlates closely with the 'inner' layer parameters *only*, even when the fence height is much greater than the depth of the log-law region. Recent work has cast some doubt on this assertion and, indeed, on the whole idea of simple correlations between drag and *any* single parameter of the upstream flow (Castro & Fackrell 1978). Certainly in the present case of square-section blocks, rather than fences, C_{D_τ} does not correlate with h/z_0. However, it does correlate with K, decreasing as K decreases. (K does not itself correlate with h/z_0 since, for F1L and F2L, the block extends beyond the log-law region.) It should be noted that blockage corrections (e.g. like those suggested on an empirical basis by Castro & Fackrell (1978) for fence flows) do not alter the general trend in the present data.

The couple, C, acting on the blocks also decreases with increasing $1/K$; this is discussed in § 4.

3.2. *The wake flow*

A considerable amount of mean velocity and turbulence data was accumulated during the course of the work and a complete presentation of all the basic data would be inappropriate. As typical examples of both the general measurement repeatability and the relaxation of the wake flow a subset of the data for F2L is shown. It will be seen in § 4, and, indeed, could be anticipated from inspection of table 3, that this flow lies between F1S and F1L as far as trends are concerned.

Figure 7 shows the profiles of mean velocity, shear stress and the three normal stresses, compared with the basic boundary-layer flow, BL2, at $x/h = 18{\cdot}0$. Results for U and $\overline{u^2}$ were of course available from both orientations of the crossed-wire probe and show reasonable agreement. The mean velocity measurements, when corrected for turbulence effects according to the work of Tutu & Chevray (1975), agree closely with single hot-wire measurements and the crossed-wire $\overline{u^2}$ measurements are a little lower than single wire measurements (not shown), in line with the expected turbulence effects on the two probe geometries. In all subsequent figures and results where crossed-wire mean velocity measurements are used directly or indirectly, these have been corrected for turbulence effects, although it turned out that the general trends in the data were not significantly altered by such corrections. It is also noteworthy that in the few cases where pulsed-wire mean velocity measurements were made in regions where the corrected hot-wire measurements were expected to be reasonably accurate the results generally differed by less than about 1 % of U_0, the local free-stream velocity.

Figure 8 shows the way in which the profiles of mean velocity, shear stress and longitudinal turbulent intensity gradually recover to the basic boundary-layer profiles. For clarity results at only five x/h stations are presented, though measurements were made at ten. Some initial observations will be made here, prior to a fuller analysis and discussion in §§ 4 and 5. Firstly and not unnaturally it is clear that the wake is

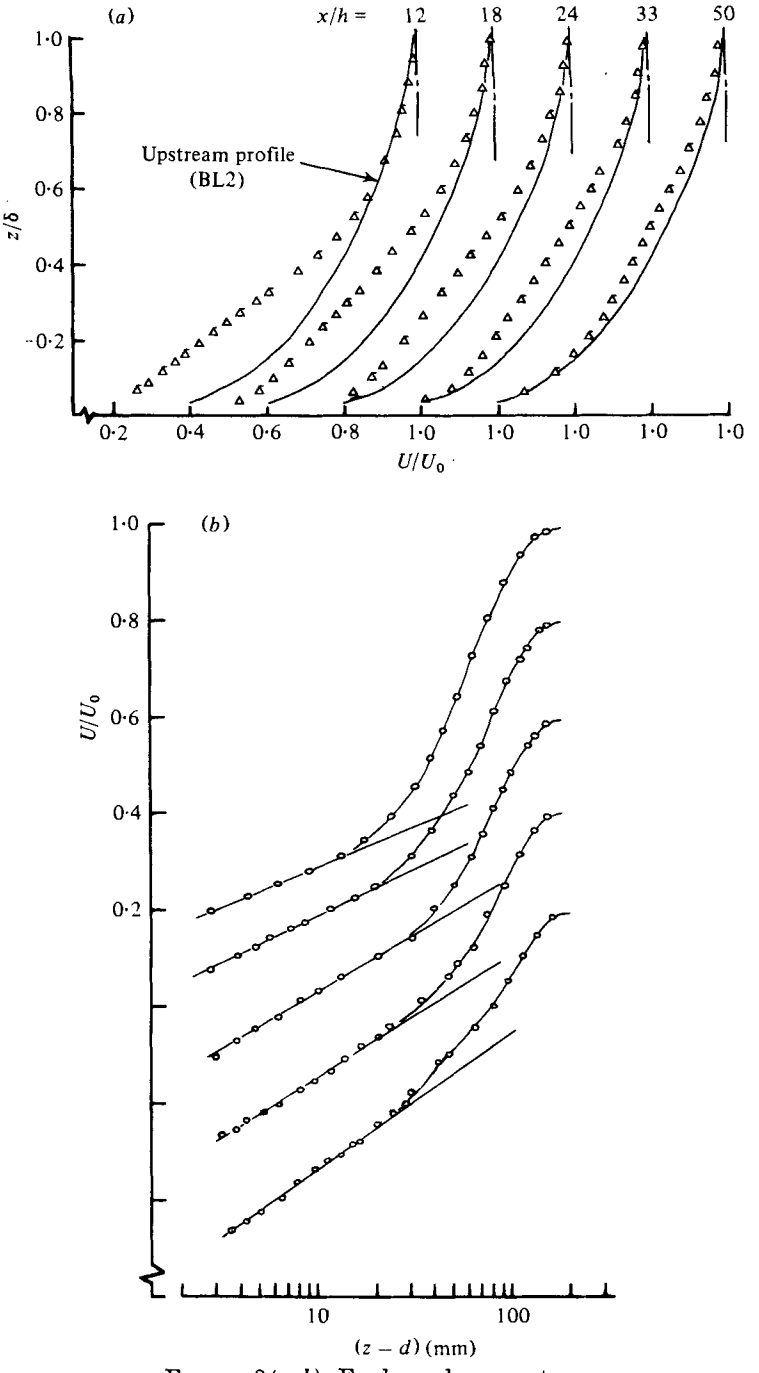

FIGURE 8 (*a*, *b*). For legend see next page.

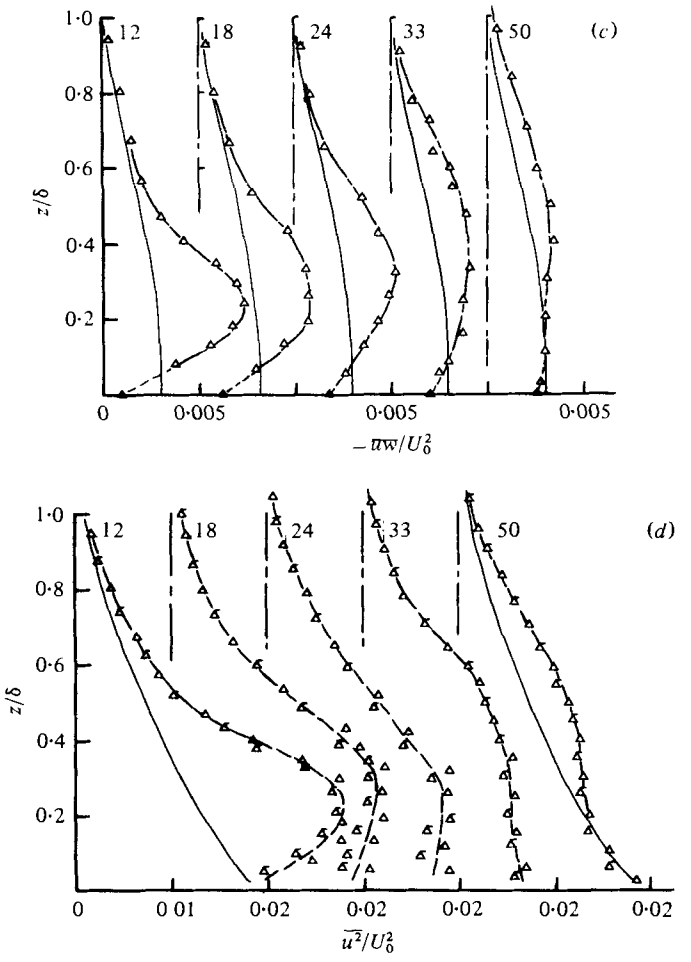

FIGURE 8. Typical results for F2L, $x/h = 12$–50. Symbols as in figure 7(*a*). (*a*) Mean velocity. (*b*) Logarithmic plots of mean velocity. (*c*) Shear stress. Solid symbols are values estimated from the log plots. (*d*) Normal stresses.

evidenced by a velocity deficit and increases in shear stress and turbulence intensity. Near the wall, however, the shear stress is actually *lower* than its undisturbed value; it must, of course, be zero at or near reattachment (around $x/h = 10$ in this case).

The recovery process appears to be most rapid at the lower velocity edge of the wake – the near wall region. At $x/h = 50$ the measurements below $y/\delta_0 \simeq 0{\cdot}15$ are virtually indistinguishable from the undisturbed boundary-layer profiles, but elsewhere there is still a clear wake region which has, in fact, grown at its outer edge to fill the entire boundary layer. A series of careful single hot-wire measurements in the near-wall region at each axial station was undertaken in an attempt to obtain an independent measure of the wall shear stress. With the assumption that the zero plane displacement, d, was the same everywhere as it was in the basic boundary layer (BL2), straight line fits to the data plotted in log-law form (figure 8*b*) led to estimates of the wall shear stress, and these are included in figure 8(*c*). However, such a process is, for rough walls, a hazardous procedure – with *no* prior assumptions about zero plane

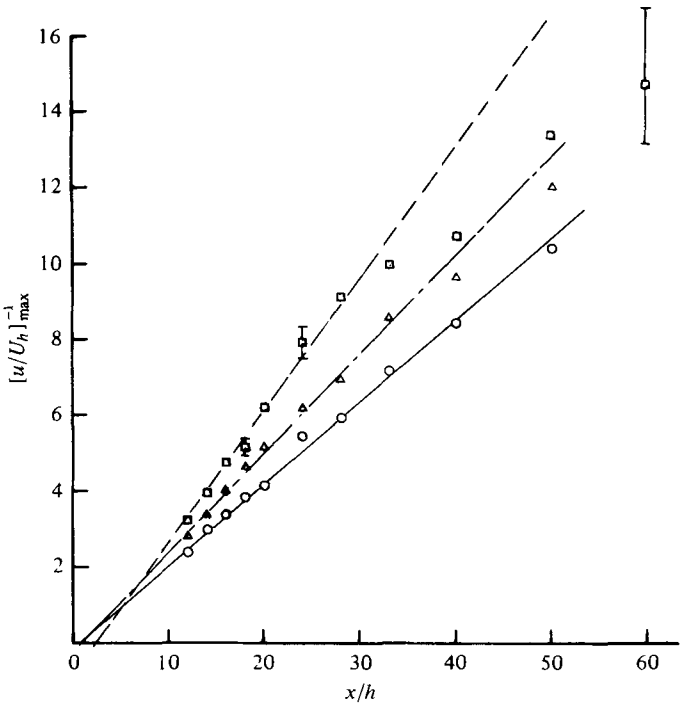

FIGURE 9. Decay of maximum velocity perturbation. ○, F1L; △, F2L; □, F1S; scatter bars correspond to an error of $\pm\frac{1}{4}\%$ in u/U_0.

displacement, wall shear stress or roughness length it is usually possible to fit a whole variety of equally satisfactory straight lines to the necessarily imperfect experimental data (Castro 1978*b*). In the present case, with the above procedure, the roughness length, z_0, appeared to be rather lower than the 0·32 mm measured in the undisturbed boundary layer, although increasing with x (to about 0·22 mm at $x/h = 50{\cdot}0$). It could be argued that z_0 is more likely to be constant than d, so the most that can be said is that the estimated wall shear stresses, whilst probably not very accurate, are not inconsistent with the crossed-wire measurements.

Similar general features of the wake flow were evident for F1L and F1S although the magnitudes of the perturbations and the rates at which they decayed were different. With the raw results, like those shown in figures 7 and 8, for all three cases it is possible to investigate the perturbation flows in some detail, and these are now compared with the theoretical results of CHJ.

4. Derived quantities – comparisons with theory

4.1. *The mean velocity perturbations*

One of the basic results of the theory of CHJ is that vertical profiles of the perturbation velocity, u, defined as the difference between the velocity in the wake and the velocity in the undisturbed boundary layer at the same height, have a self-preserving form in the region away from the wall, given by

$$-\frac{u}{U_h}.(\bar{x}) = \frac{\tilde{C}}{Kh^2U(h^2)}.F(\eta, n), \tag{1}$$

where $\tilde{C}$ is a constant, $\eta = (y/h).(K\bar{x})^{-1/(n+2)}$, $\bar{x} = (x-a)/h$, a is a virtual origin and F contains confluent hypergeometric functions and is virtually independent of the small changes in the power law exponent, n, resulting from different upstream boundary layers. The maximum value of the velocity perturbation should therefore be inversely proportional to $\bar{x}$, and in figure 9 $(u/U_h)^{-1}_{\max}$ is plotted against x/h for all three cases. Using the resulting values for a and the appropriate values for K (table 2) the profiles are plotted in the self-similar form in figure 10. For reasons discussed later the straight lines in figure 9 have been biased towards the data at the lower end of the x/h range, where necessary. Typical scatter bars resulting from possible errors in u/U_0 of $\frac{1}{2}\%$ are included in figure 9 and, since u/U_0 is itself quite small at large x, the uncertainties obviously increase with increasing x. The theoretical self-preserving profiles can be obtained by fixing the disposable constant, $\tilde{C}$, in equation 1 so that the maximum velocity deficit is equal to the measured value. Figure 10 includes the resulting profiles and the appropriate values of $\tilde{C}/h^2U(h)^2$ are given in tables 2 and 3. There is a considerable region of each wake which does exhibit the expected self-similar behaviour away from the wall region but clearly the far wake, particularly for F1S, is not well predicted. As K increases it seems that the rate of decay of the velocity deficit begins to fall below the $\bar{x}^{-1}$ rate at smaller and smaller $\bar{x}$. Even for F1S, however, the predictions seem satisfactory up to $x/h \simeq 30$, which is further downstream than the extent of the only previously reported experiments of similar type (CHJ). These results are discussed further in § 5.

In the wall region of the wake flow, the perturbation velocity is not expected to have the self-similar form of equation (1), mainly because the assumption of a constant perturbation eddy viscosity [used in the derivation (1)] was not thought to be adequate in such a region. CHJ therefore derived a separate solution for this wall region by assuming it to be in equilibrium, so that

$$u = \frac{u_x F(\bar{x})}{\kappa} \ln (z/z_0),$$

where u_x and $F(\bar{x})$ are found by matching u and the perturbation shear stress, τ_{xy}, with the self-preserving solution of the mixing region which forms the outer boundary of the wall region. This led to

$$\frac{u}{U(h)}.\bar{x} \simeq \left[\frac{u}{U(h)}.\bar{x}\right]_{\eta_0} \frac{\ln \eta + \ln (l/z_0)}{\ln \eta_0 + \ln (l/z_0)}, \tag{2}$$

where $l/h = (K\bar{x})^{1/(n+2)}$ and η_0 is the value of η at which the gradient of $u\bar{x}/U(h)$ vanishes, i.e. where $u\bar{x}/U(h)$ reaches its maximum value. A direct implication of this is that the velocity deficit in the wall region decays more slowly than $\bar{x}^{-1}$ since, at a fixed η, the right-hand side of equation 2 increases with increasing $\bar{x}$ (because l, a measure of the overall wake width, increases with $\bar{x}$). The theoretical wall region profiles are included in figure 10 (*c*) for $x/h = 12$ and 50, demonstrating this behaviour. Now, by contrast, it is clear that the data, although somewhat scattered in this region because the experimental errors are rather higher than elsewhere, exhibits an entirely opposite trend, at least in the axial region where the self-preserving solution seems adequate. The velocity deficit actually decays *more* rapidly in this wall region than elsewhere, as was originally noted in § 3.2. This, also, will be discussed in § 5.

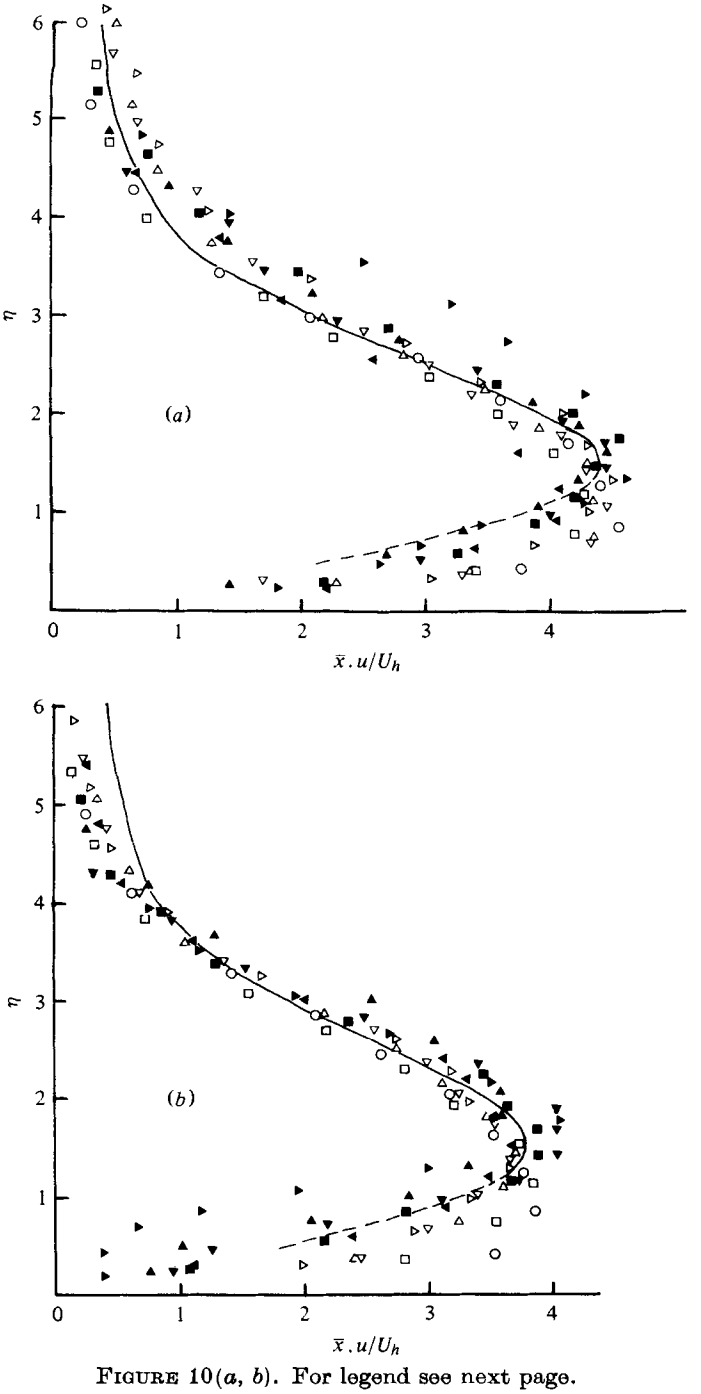

FIGURE 10(*a*, *b*). For legend see next page.

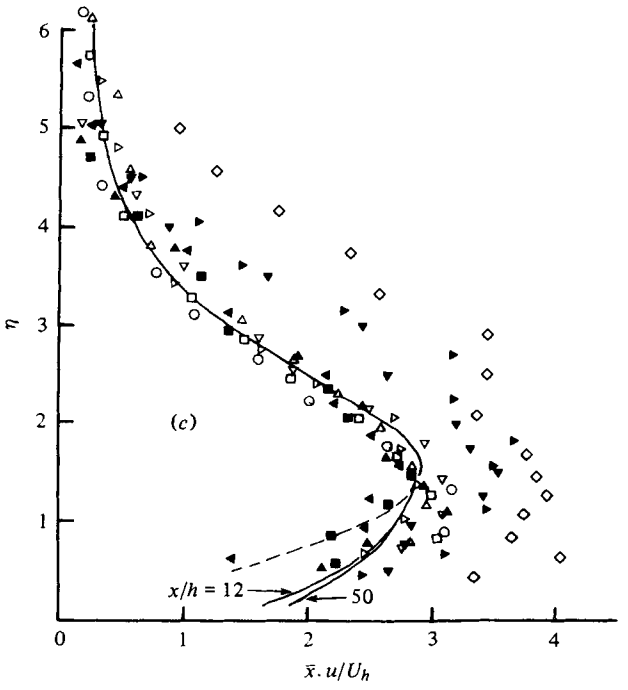

FIGURE 10. Velocity deficit profiles. x/h: ○, 12; □, 14; △, 16; ▽, 18; ▷, 20; ◀, 24; ■, 28; ▲, 33; ▼, 40; ▶, 50; ◇, 60; ——, CHJ theory. (*a*) F1L; (*b*) F2L; (*c*) F1S.

Two further points are worth noting at this stage. Firstly, CHJ point out that since $F(\eta, n)$ is virtually independent of n in the range of practical interest $(u/U_h)_{\max} . \bar{x}$ should be roughly inversely proportional to K, provided that $\tilde{C}/h^2U(h)^2$ is dependent mainly on obstacle geometry. In the present case this latter parameter decreases by only about 10 % for a roughly fourfold increase in surface roughness (see table 2 or 3), and the slope, m, of the $(u/U_h)^{-1}_{\max}$ *vs.* x/h lines in figure 9 is plotted against $1/K$ in figure 11. The data is not inconsistent with this particular implication of the theory. Included in figure 11 is the single data point available from the experiments of CHJ. Since their wake was also produced by a square-section block the good agreement is not surprising. Their corresponding values for K and $\tilde{C}/h^2U(h)^2$ were 0·05 and 0·8, respectively (cf. table 2).

A further result of the theory is that the wake constant, $\rho\tilde{C}$, is equal to the sum of the couple on the obstacle and an integral of the pressure field on the surface near the body. A comparison of the values of $\rho\tilde{C}$ and C for the three flows (table 3) leads to the interesting conclusion that not only is $\rho\tilde{C} > C$ as the theory predicts but the relative contribution to $\rho\tilde{C}$ from the surface pressures near the body decreases as K increases; for F1S ($K \sim 0{\cdot}045$) $\rho\tilde{C}/C$ is about 5·1 but it drops to about 2·9 for F1L ($K \sim 0{\cdot}068$). This is not, perhaps, a surprising result because, although quantitative static pressure measurements within the wake were not made, it was clear that increasing K reduced the relative extent of the surface pressure perturbations both upstream and downstream of the body; the length of the separated region behind the obstacle was indicative of this: for F1L it was about $11h$ but it was only about $9h$ for F1S.

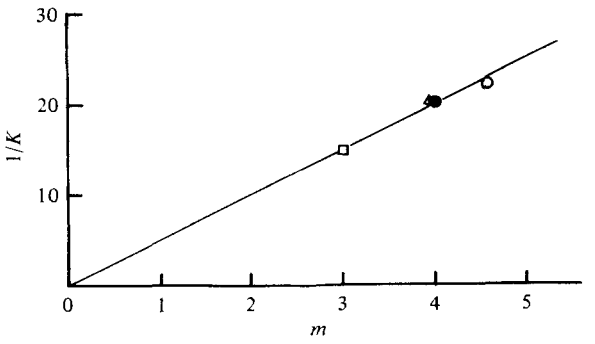

FIGURE 11. The relationship between $1/K$ and m. ○, F1L; △, F2L; □, F1S; ●, CHJ results.

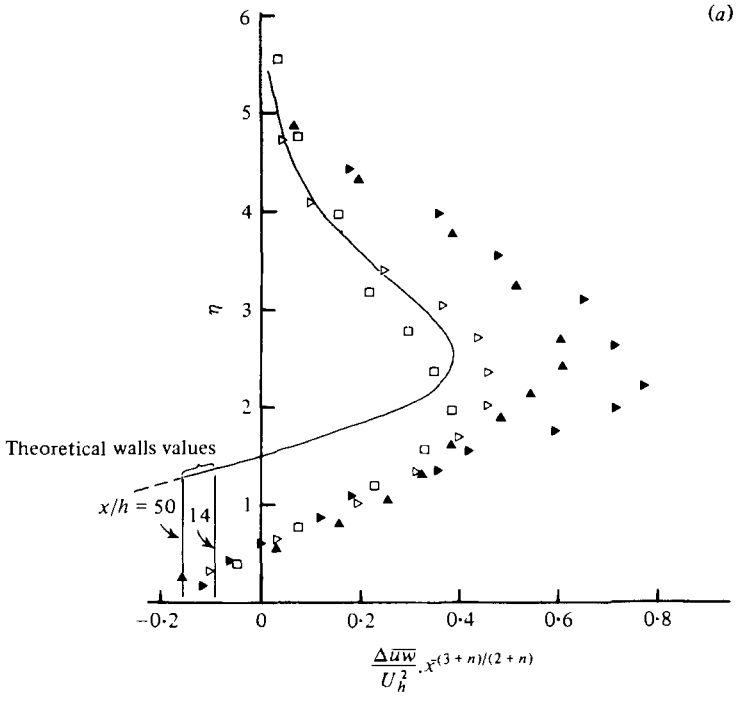

FIGURE 12(*a*). For legend see next page.

4.2. *Perturbations of the turbulence field*

The perturbation shear stress in the wake is $\Delta(-\overline{uw})$, defined as the increase in $-\overline{uw}$ in the wake above that in the boundary layer. Corresponding to equation (1) the theoretical variation of $\Delta(-\overline{uw})$ in the region away from the wall is

$$\frac{\Delta(-\overline{uw})}{U_n^2}.\bar{x}^{(3+n)/(2+n)} = \frac{\tilde{C}}{K^{1/(2+n)}h^2U_h^2}.\frac{dF(\eta,n)}{d\eta}.$$

The data is plotted in this expected self-preserving form in figure 12 for all three flows, and compared with the theoretical profile obtained by using the same value for $\tilde{C}$ used in the corresponding mean velocity comparisons (tables 2 and 3 and see § 4.1). For

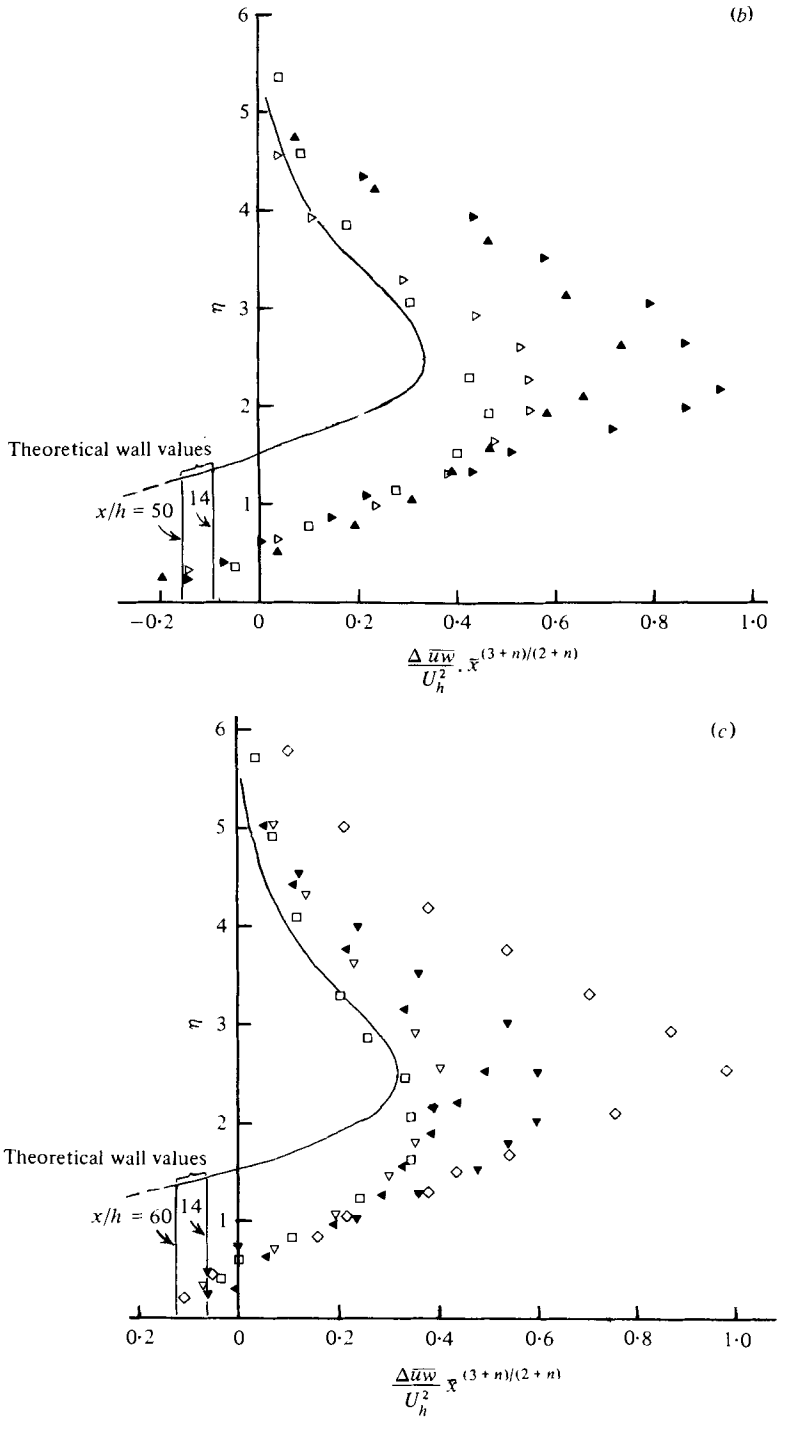

FIGURE 12. Shear stress perturbation profiles. Symbols as in figure 10. (*a*) F1L; (*b*) F2L; (*c*) F1S.

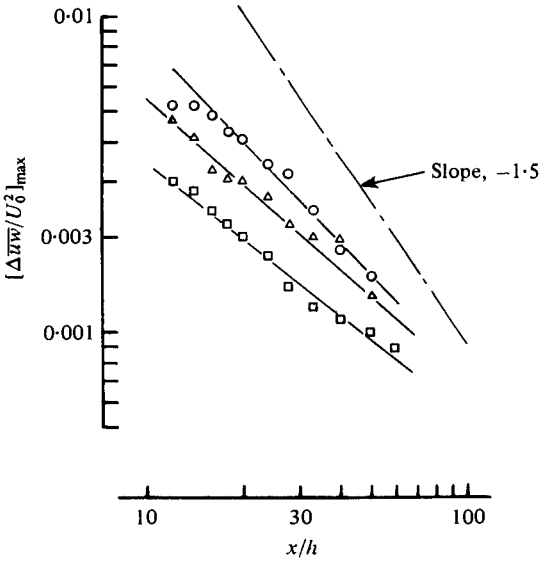

FIGURE 13. Decay of maximum shear stress perturbation. Symbols as in figure 11.

the present values of n (0·19 and 0·23) the maximum value of $dF(\eta, n)/d\eta$ was about 0·113, compared with the 0·117 obtained by CHJ with $n = 0{\cdot}125$.

The maximum shear stress increase has about the expected magnitude just downstream of the separated region ($\sim x/h = 12$) but clearly decays significantly less rapidly than the theory suggests. Furthermore, a plot of $[\Delta(-\overline{uw})/U_0^2]_{max}$ *vs.* x/h indicates that the rate of decay decreases with increasing K, figure 13, in line with the trends described in the previous section which indicated that the rate of decay of the velocity deficit decreased with increasing K.

In the wall region the assumption of equilibrium with a matching of solutions in this and the mixing region leads to a constant perturbation shear stress with a magnitude of

$$\frac{\Delta - \overline{uw}}{U_h^2} = \frac{2\kappa(U_\tau/U_0)\,[\bar{x}\,.\,u/U_h]_{max}}{\bar{x}\ln\left[(h/z_0)\,.\,\eta_0(K\bar{x})^{1/(n+2)}\right]}$$

(a rearranged form of the expression given by CHJ). This theoretical result is included for typical values of x/h in figure 12, for all the flows. As in the case of the theoretical velocity perturbation, the implication is that the perturbation shear stress decays less rapidly in the wall region whereas, in fact, the data indicates that it decays rather more rapidly. Indeed, the data actually collapses, within experimental accuracy, on the similarity plots (figure 12) in just the region where the theory predicts that it should not. The perturbation shear stress therefore decays approximately like $\bar{x}^{-\frac{3}{2}}$ in the wall region, but significantly slower elsewhere (figure 13). The wall region solution is only valid as $y \to 0$ since, as CHJ recognized, 'inertial effects were ignored in its derivation'. Good agreement was not, therefore, expected in this region but it is interesting that the magnitude of the predicted wall shear stress is not seriously in error.

Although the turbulent shear stress is reduced below the boundary-layer value in

the near wall region the normal turbulent stresses all increase so that, as discussed later, the turbulence structure is rather different from an equilibrium flow. However, away from the wall the increases in turbulence intensities are very similar in magnitude to the increases in shear stress. For F1S, for example, the maximum increase in turbulence energy expressed as a fraction of the upstream value, $[\Delta\overline{q^2}/\overline{q^2}]_{\max}$, is about 0·9 at $x/h = 14$, compared with a corresponding increase in shear stress of about 1·3. For F1L the corresponding figures are about 2·1 and 2·3. In addition, the rate at which the perturbation intensities decay is very close to the rate of decay of the shear stress perturbations, so that for F1L, for example, $[\Delta\overline{q^2}/\overline{q^2}]_{\max}$ and $[\Delta - \overline{uw}/\overline{uw}]_{\max}$ are about 0·8 and 1·0, respectively, by $x/h = 50$.

Some of the implications of all these results are discussed in the following sections.

5. Further discussion

5.1. *The reattachment region*

The characteristics of the relaxing flow downstream of reattachment must depend, to some extent at least, on the nature of the flow in the region of reattachment and, indeed, on the flow in the separated shear layer and the recirculating region which it bounds. Only insofar as this region of the flow is affected by the upstream boundary-layer characteristics will the relaxing region downstream be so affected. It is therefore important to have some understanding of the flow near reattachment. Unfortunately this is just the region where it is most difficult to make accurate measurements, but some fairly definitive statements are possible, nevertheless.

The separated shear layer must, at least close to separation whether this is at the upstream or the downstream edges of the body, have characteristics similar to a plane mixing layer. This is demonstrated by, for example, the data of Tani, Iuchi & Komoda (1961) and, more recently, Chandrsuda (1975) in the case of flow over a backward facing step. However, the distortion of the shear layer as it approaches reattachment is likely to be considerable and, in fact, Bradshaw & Wong (1972), in a review of previous experiments with some of their own, concluded 'that the flow just downstream of reattachment bears very little resemblance to a plane mixing layer or any any other sort of thin shear layer. . . '.

Now it is clear that the flow down a rearward facing step will differ in detail from a flow, like the present ones, involving *two* separations. In most of the former experiments, $h \gg \delta$ or, at least, $h \nless \delta$, whereas in the present case $h \ll \delta$. Using Bradshaw & Wong's terminology the present perturbation is a 'weak' one compared to the step flow. As far as the separated shear layer itself is concerned, however, it is probably perturbed more strongly in the present case, as discussed below. Similar trends in the two flows might be expected, nevertheless.

For a backward facing step flow Bradshaw & Wong found that near the region of maximum shear stress in a plane just downstream of reattachment the ratio of the mixing length, $l \equiv (-\overline{uw})^{\frac{1}{2}}/(\partial U/\partial z)$, to the dissipation length scale, L, was considerably greater than its value in the central region of a plane mixing layer. This was caused principally by a sudden decrease in the turbulence length scale, L, as the shear layer bifurcated at reattachment. Their reasoning was largely intuitive because no direct length scale measurements were made. Etheridge & Kemp (1978), as a result of measurements in a similar flow, made the same point.

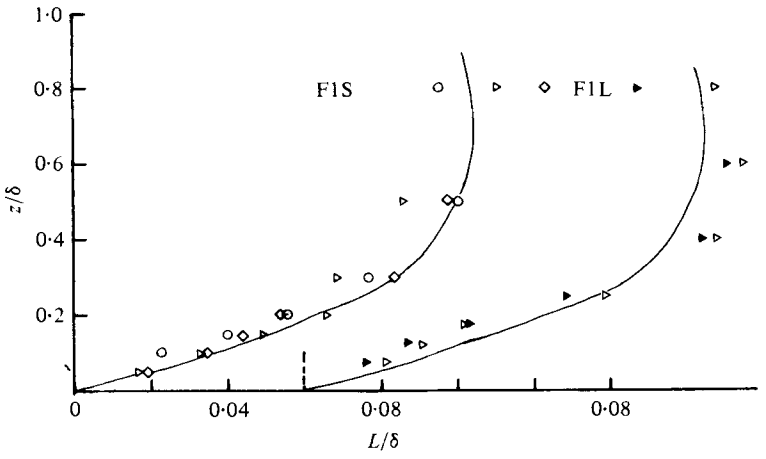

FIGURE 14. Dissipation length scale. x/h: ○, 12; ▷, 20; ◇, 60 (F1S); ▷, 20; ▶, 50 (F1L). ——, upstream profile (BL1).

In the present case L was measured (as described in § 2.3) at a few stations downstream of reattachment and it is interesting to compare the results with the conclusions of Bradshaw & Wong. Figures 14 and 15 show the variations of L and l/L for F1S and F1L at various x/h, compared with the profiles measured in the undisturbed boundary layer and also with the profile in a plane mixing layer (e.g. Castro 1973). For the latter profiles the mixing layer width has been scaled so that it roughly corresponds to the width of the perturbation stress profiles at $x/h = 12$. In these flows L seems to be reduced so much from the plane mixing layer levels that it does not increase with y more rapidly than it would in a log-law region (figure 14), unlike the behaviour suggested by Bradshaw & Wong. However, for F1L, l does increase more rapidly than κy so that, although for F1S it does not, in both cases there *are* significant increases in l/L (figure 15). Etheridge & Kemp (1978), like Bradshaw & Wong, also found that l increases near the wall at a faster rate than in an equilibrium wall layer, but their data did not allow definite conclusions about the behaviour of L, which, unlike l, is a true turbulence length scale. However, the indications were that L tended to decrease near reattachment, so the present work is in line with the previous weight of evidence in suggesting that turbulence length scales are reduced as reattachment is approached. It may also be noted here that there was no dip below the log-law in the mean velocity profiles of the kind found by the latter authors who argued that the dip was maintained by the rapid rise in L.

Figure 15 also demonstrates that the distorting effects of reattachment on the shear layer are considerably greater for F1L than for F1S. Bradshaw & Wong (1972) argue that this 'distortion... depends on what fraction of the mass flow is deflected upstream to supply the entrainment' (required by the mixing layer). Since the length and velocity scales of the flow just outside the separated mixing layer must be closer in magnitude to those in the mixing layer itself for F1S than they are for F1L (because h/δ is only about 0·07 in the former case) the external flow may have more effect on the mixing layer in F1S, leading to a smaller portion of the layer having to be deflected upstream at reattachment. The higher base pressure in this case (figure 6) certainly implies a relatively weaker reversed flow region. This would explain why the greater

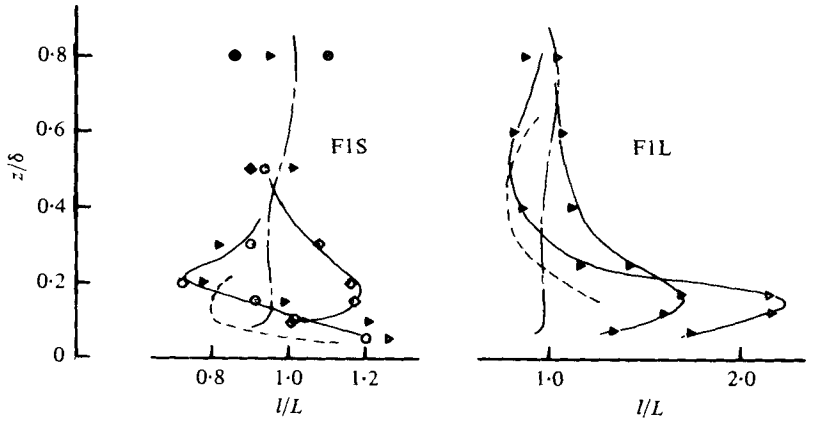

FIGURE 15. Ratio of mixing length to dissipation length scale. Symbols as in figure 14; —·—, upstream profile; – – –, mixing layer profile.

effect on the turbulence structure of the separated mixing layer occurs for larger values of, say, $1/K$ – the turbulence Reynolds number of the body.

Further indications of the turbulence characteristics just downstream of reattachment are given by the plots of the 'structure functions', $\overline{uw}/\overline{q^2}$ and $\overline{uw}/(\overline{u^2}.\overline{w^2})^{\frac{1}{2}}$, in figure 16. These are compared with the profiles in the undisturbed boundary layer, which are typical of zero-pressure-gradient boundary layers. Even as early as $x/h = 14{\cdot}0$, the turbulence stresses have relative magnitudes quite close to the boundary layer values, except of course in the near wall region where the shear stress is still very small. Chandrsuda (1975) found very similar values for the structure functions near reattachment downstream of a rearward facing step. Although the magnitudes of the individual turbulence stresses measured by Etheridge & Kemp (1978) are rather larger than those found by previous workers with the same geometry (e.g. Chandrsuda 1975; Baker 1977), their structure functions were similar, around reattachment, to the present, and previous, data. For F1L, in which the shear layer apparently suffers the greatest distortion, the structure functions are not much lower than the plane mixing layer values – about 0·15 and 0·55 for $\overline{uw}/\overline{q^2}$ and $\overline{uw}/(\overline{u^2}.\overline{w^2})^{\frac{1}{2}}$, respectively; it should be said, however, that quite large extra strain rates are necessary to produce large and prolonged effects on the structure functions.

5.2. *The relaxing flow*

Discussion of the decaying, perturbed flow downstream of reattachment begins with a consideration of the flow generated by the smaller of the two bodies (flow F1S), largely because in this case the assumptions used by CHJ are likely to be most closely satisfied. Using the present data for F1S, the measured eddy viscosity, $\nu_\tau \equiv \overline{uw}/(\partial U/\partial z)$ at $x/h = 12$, 28 and 60 is shown in figure 17(*a*). In their analysis, CHJ assumed that the eddy viscosity in the mixing region could be represented by

$$\nu_0(h)\,[1 + (\partial u/\partial y)/(\partial U/\partial y)]$$

but it is obvious that the variations of ν_τ could not be predicted by simple formulae of this type – which is included in the figure. In fact, the eddy viscosity profiles are

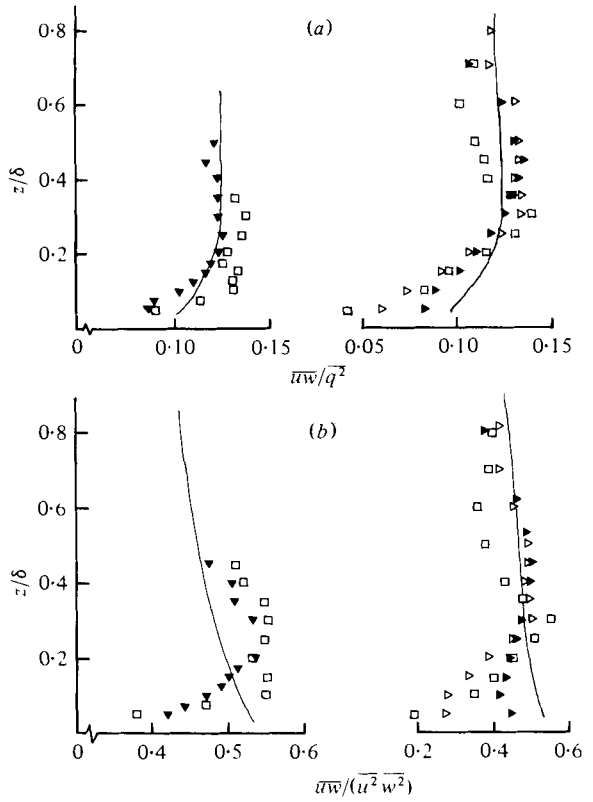

FIGURE 16. Turbulence structure functions. x/h: □, 14; ▼, 40 (F1S); □, 14; ▷, 20; ▶, 50 (F1L). (*a*) $\overline{uw}/\overline{q^2}$. (*b*) $\overline{uw}/(\overline{u^2}.\overline{w^2})^{\frac{1}{2}}$; the second figure has a different horizontal length scale.

closer to the upstream values than the CHJ assumption. Furthermore, since the significant variations in l/L described earlier imply that shear stress transport terms must vary with x, it seems likely that *any* eddy viscosity relation will be unsuccessful in predicting the total flow. It would, nevertheless, be interesting to see how well the more sophisticated eddy viscosity models (e.g. the common two-equation models: Launder & Spalding 1972) fare in predicting the downstream flow using measured data just downstream of reattachment as upstream boundary conditions.

With simple assumptions about the response of the eddy viscosity to extra strain rates (see figure 17*a*), CHJ derived a perturbation eddy viscosity, $\nu_p = 2\nu_0(h)$ and this was the value used to link the perturbation mean velocity and shear stress fields in their prediction of the *perturbed* flow. It is compared with the experimental data in figure 17(*b*). Since the points of zero $\Delta(-\overline{uw})$ and $\partial u/\partial y$ do not coincide, there are discontinuities in ν_p at the point of maximum velocity deficit, but nevertheless it is clear that a constant perturbation eddy viscosity is not an adequate assumption. Indeed, since the data of figure 17 clearly demonstrate that the perturbation mean velocity decays more rapidly than the perturbation shear stress (as previously seen in § 4) it seems probable that no eddy viscosity relation for the *perturbation* flow would be satisfactory, any more than it would for the total flow.

Now the predicted mean velocity is generally less sensitive than the turbulence

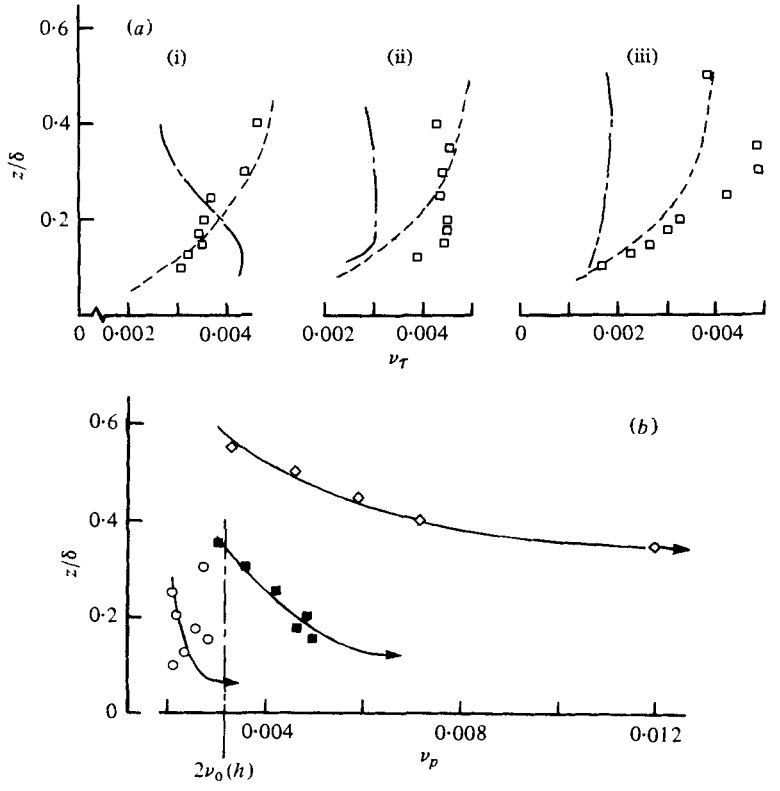

FIGURE 17. (*a*) Eddy viscosities, F1S. □, $\overline{uw}/(\partial U/\partial y)$; – – –, upstream profile; —·—, $\nu_m = \nu_0(h)\,[1+(\partial u/\partial y)/(\partial U/\partial y)]$. (i) $x/h = 12$; (ii) 28; (iii) 60. (*b*) Perturbation eddy viscosity, $\Delta(-\overline{uw})/(\partial u/\partial y)$, F1S. —○—, $x/h = 12$; —■—, $x/h = 28$; —◇—, $x/h = 60$.

quantities to the exact nature of the turbulence model and since, in addition, it so happens that $2\nu_0(h)$ is not too far in magnitude from the measured ν_p in the early part of the wake ($x/h \gtrsim 28$, say), the mean velocity perturbations are reasonably well predicted in this region (figure 10 and § 4.1), whilst the shear stress perturbations are, of course, less well predicted.

Consider now flows F1L and F2L, generated by the larger of the two blocks. It is at first sight surprising that, at least as far as the mean velocity perturbations are concerned, the wake decay is apparently better predicted than it is for F1S (figures 9 and 10), despite the fact that the shear layer turbulence after separation is more highly distorted (e.g. figure 15). The maximum velocity deficit decay rate does not decrease as $\bar{x}$ increases, as it does for F1S. However, for F1L and F2L the wake practically fills the boundary layer by about $x/h = 40$ so that the CHJ assumption that δ is not a relevant length scale cannot be very satisfactory. Near reattachment we might, perhaps, expect the theory to give reasonable predictions, but beyond, say, $x/h = 20$, by which time the wake region extends over at least $0{\cdot}7\delta$, the relatively large scale eddies of the outer region of the boundary layer will assume increasing importance. Indeed, they will provide the strongest mechanism for vertical diffusion of turbulence energy and shear stress so that the wake decay is likely to proceed rather faster. Since, in their absence, the decay would begin to slow down in this region (cf. F1S, figure 9),

the fact that the x^{-1} decay rate is actually maintained over the whole measured extent of the wake is therefore likely to be a result of the opposing effect of two inadequate assumptions in the theory. Convincing substantiation of these conclusions would necessitate a closer investigation of the turbulence structure than was possible in the present study. In particular, it would be instructive to study in detail a flow like F1S, with measurements even further downstream where, if the above arguments are valid, the decay rate might be expected to rise again, although it must be said that CHJ thought that 'to second order in $u/U(h)$, it is likely that $u \neq 0$ as $x \to \infty$'.

A referee has suggested that, if, like grid turbulence, the turbulence perturbations produced by the body and reattachment region decay like x^{-1}, this may actually dominate over the locally produced turbulence which the CHJ theory shows to fall off like $x^{-\frac{5}{3}}$. Certainly the perturbation stresses do fall off less rapidly than $x^{-\frac{5}{3}}$ (e.g. figure 13). Rough calculations for F1L at $x/h = 20$ and $y/\delta = 0{\cdot}3$ show that the time scale for advection of turbulence perturbations (say, $\Delta\overline{q^2}/U\partial\Delta\overline{q^2}/\partial x$, suitably normalized) is typically only one quarter of the local production time scale (say, $\Delta\overline{q^2}/\Delta(-\overline{uw})\,\partial u/\partial y$, similarly normalized) which is itself an order of magnitude greater than the mean flow time scale (say, $\overline{U}/x$, where $\overline{U}$ is an average velocity at $y/\delta = 0{\cdot}3$). The advection time scale is possibly small enough to suggest that decay of locally produced turbulence can be ignored compared with the decaying upstream turbulence but since it and the production time scale are both large compared with the mean flow time scale the possibility of precise establishment of a self-preserving perturbation flow is probably rather remote.

However, what is clear is that the wake flow is, like the flow near reattachment, sufficiently complicated to ensure that theories or, for that matter, numerical predictions which use eddy viscosity turbulence models are not likely to be successful in predicting the total flow, although they might give seemingly adequate results in limited regions.

One result of the theory which should not, in principle, depend on the assumed turbulence model, is that the rate of decay of the wake is inversely proportional to a ratio $(1/K)$ of inertial stresses to turbulence shear stresses in the upstream flow at, say, the height of the body. The experimental data do seem to confirm this (figure 11) and it appears that the primary effect of this ratio is on the distortion of the separated shear layer up to reattachment. Downstream of this, the wake relaxation is slowest in the case of the greatest distortion (F1L). On the other hand, in the wall region the velocity perturbations decay *more* rapidly for F2L than for F1L (figures 10*a* and *b*) but this is almost certainly a result of the considerably rougher surface in the former case. The thickness of the region obeying the log-law grows at a similar rate in the two cases but since, at a given z, the velocity in the undisturbed boundary layer is less for the rougher surface, the perturbation velocity will, in the equilibrium wall layer downstream of reattachment, also be less.

What is, perhaps, more interesting is that the log-law region grows at about the same rate in all three cases, which agrees with the suggestion of Bradshaw & Wong (1972) that a local-equilibrium region re-establishes itself at a rate almost independent of the turbulent flow that provides its outer boundary condition.

One final comment on the overall flow is worth making. In a recent paper Crabb *et al.* (1977) suggested that in their case of a two-dimensional block mounted in a relatively thin upstream boundary layer ($h/\delta > 1$) there was considerable large scale

unsteadiness in the flow downstream of separation from the body; their measured probability distributions had a noticeable 'double-peak' shape which they interpreted as being indicative of strong unsteadiness at a particular frequency superimposed on top of the usual turbulence structure. This, of course, would make numerical steady-state predictions an even more doubtful procedure. Some probability distributions were obtained in the present flows and nowhere was there any sign of a double peak structure. The unsteadiness would, in fact, have to be particularly strong to produce such a probability density distribution but the spectral measurements also gave no indication of such behaviour; it may be that any tendency for the flow to exhibit unsteadiness is sensitive to 'free-stream' turbulence so that when $h/\delta \ll 1$, as in the present case, the unsteadiness is entirely suppressed. Further work would help to elucidate this point.

6. Conclusions

The first conclusion of this paper is that in the region of the wake not too far downstream of reattachment the velocity and turbulence perturbations decay in a manner governed largely by the characteristics of the upstream flow at, say, the body height. However, this control of the wake decay is exercised principally through the distortion effects on the separated shear layer which, to an even greater extent than in the previously studied case of flow over a backward facing step (Bradshaw & Wong 1972), are severe. Since the major effect near reattachment is to reduce the typical turbulence length scales sufficiently to imply significant transport effects farther downstream, eddy viscosity models are not adequate for predicting the relaxing flow. Whether more recently developed turbulence models based on closure of transport equations for the Reynolds stresses with some length scale equation could adequately predict the present flow remains to be seen. In this context it is interesting to note that, although Castro & Bradshaw (1976) concluded in their study of a highly curved mixing layer that even the more refined transport equations for the eddy length scale may be incapable of reproducing the observed effects, Gibson (1979) has recently been moderately successful in predicting their flow with just such a method.

The theory of Counihan *et al.* (1974), whilst it correctly indicates the way in which the wake decay changes with the upstream flow characteristics, is not sufficiently realistic to give good predictions of the total flow downstream of reattachment. The mean velocity perturbations decay initially like x^{-1}, as predicted by the theory, but this decay rate gradually decreases with increasing distance downstream although it remains noticeably more rapid than the recovery of the turbulence field. Once the wake has spread into the outer region of the boundary layer the large eddies there assist the wake decay so that, for some values of h/δ, the velocity perturbations do decay roughly at the theoretically predicted x^{-1} rate, but this is largely fortuitous. In the wall region the flow recovers rather more rapidly than elsewhere, in contrast to the theory, and in fact at a rate which does not seem to depend strongly on the outer flow.

In contrast to the case of flow over a block in a *smooth* wall boundary layer with a similar value of h/δ (Castro & Fackrell 1978) the shear layer separating from the leading edge of the block reattaches onto the top surface of the block in all the present flows. This is presumably a result of the higher turbulence levels upstream but further

work is required to determine exactly how the upstream flow controls the separated shear layer. The degree of distortion of this shear layer as it approaches reattachment downstream of the body must depend partly on whether or not it reattaches and then separates again from the body surface itself.

Finally, there was no evidence of large-scale unsteadiness in the wake, but this is no reason to suppose that in other cases, for $h/\delta > 1$ for example, such unsteadiness would not be present. In view of the possible implications for numerical prediction methods, this aspect of such flows requires further study.

Whilst it is felt that the present work is of help in understanding some of the complex turbulent flows that occur in engineering practice, there is no doubt that more detailed measurements of the turbulence structure of such flows is necessary for an understanding sufficient to develop adequate turbulence models. Indeed, even more basic data of the kind presented here would be useful if only as a 'bench mark' against which to test the results of the increasingly daring numerical predicters.

The author would like to acknowledge the assistance of Mr J. E. Pearce in undertaking the experiments which were performed at the Marchwood Engineering Laboratories of the Central Electricity Generating Board. Their permission to publish the results is therefore also acknowledged.

REFERENCES

BAKER, S. 1977 Ph.D. thesis, University of Surrey.

BRADSHAW, P. 1969 *Aero. Res. Counc. R. & M.* no. 3603.

BRADSHAW, P. 1971 *An Introduction to Turbulence and its Measurement.* Pergamon.

BRADSHAW, P. 1975 *J. Fluids Engng, Trans. A.S.M.E.* **97**, 146.

BRADSHAW, P. & WONG, F. Y. F. 1972 *J. Fluid Mech.* **52**, 113.

CASTRO, I. P. 1973 Ph.D. thesis, Imperial College, London.

CASTRO, I. P. 1978*a* The numerical prediction of recirculating flows. In *Proc. Conf. on Numerical Methods in Laminar and Turbulent Flows*, p. 329. Pentech Press.

CASTRO, I. P. 1978*b* *C.E.G.B. Rep.* R/M/N1006.

CASTRO, I. P. 1979 Numerical difficulties in the calculation of complex turbulent flows. In *Turbulent Shear Flows. I* (ed. Durst *et al.*). Springer.

CASTRO, I. P. & BRADSHAW, P. 1976 *J. Fluid Mech.* **73**, 265.

CASTRO, I. P. & FACKRELL, J. E. 1978 *J. Ind. Aero.* **3**, 1.

CASTRO, I. P. & ROBINS, A. G. 1977 *J. Fluid Mech.* **79**, 307.

CHANDRSUDA, 1975 Ph.D. thesis, Imperial College, London.

COLES, D. 1956 *J. Fluid Mech.* **1**, 191.

COUNIHAN, J. 1969 *Atmos. Environ.* **3**, 197.

COUNIHAN, J., HUNT, J. C. R. & JACKSON, P. S. 1974 *J. Fluid Mech.* **64**, 529.

CRABB, D., DURÃO, D. F. G. & WHITELAW, J. H. 1977 Velocity characteristics in the vicinity of a two-dimensional rib. *Paper presented at the 4th Brazilian Cong. Mech. Eng.*

ETHERIDGE, D. W. & KEMP, P. H. 1978 *J. Fluid Mech.* **86**, 545.

GIBSON, M. 1979 (To appear).

GOOD, M. C. & JOUBERT, P. N. 1968 *J. Fluid Mech.* **31**, 547.

LAUNDER, B. E. & SPALDING, D. B. 1972 *Mathematical Models of Turbulence.* London: Academic Press.

LAWN, C. J. 1971 *J. Fluid Mech.* **48**, 477.

PETERKA, J. A. & CERMAK, J. F. 1975 Turbulence in building wakes. In *Proc. 4th Int. Conf. on Wind Effects on Buildings and Structures, Heathrow.* Cambridge University Press.

PLATE, E. J. 1964 *A.S.M.E. Paper* no. 64-FE-17.

RAJU, R. K. G., LOESER, J. & PLATE, E. J. 1976 *J. Fluid Mech.* **76**, 383.

ROBINS, A. G. 1979 *J. Ind. Aero.* **4**, 71.

SHIEH, C. F., FROST, W. & BITTE, J. 1976 *Rep.* under NAS8-29584, *Atmosph. Sci. Div. Univ. Tennessee Space Inst.*

TANI, I., IUCHI, M. & KOMODA, H. 1961 Aero. Res. Inst. University of Tokyo Rep. no. 364.

TOWNSEND, A. A. 1965 *J. Fluid Mech.* **22**, 773.

TUTU, N. K. & CHEVRAY, R. 1975 *J. Fluid Mech.* **71**, 785.